A tree-topology preserving pairing for 3D/2D registration

Thomas Benseghir, Grégoire Malandain, Régis Vaillant

A Tree-Topology Preserving Pairing for 3D/2D Registration

Thomas Benseghir*[1,2], Grégoire Malandain†[2], and Régis Vaillant‡[1]

[1]GE-Healthcare, 78530 Buc, France
[2]INRIA, 06900 Sophia Antipolis, France

3 April 2015

Abstract

Purpose: Fusing pre-operative and intra-operative information into a single space aims at taking advantage of two complementary modalities and necessitates a step of registration that must provide good alignment and relevant correspondences. This paper addresses both purposes in the case of 3D/2D vessel tree matching.

Method: We propose a registration algorithm endorsing this vascular tree nature by providing a pairing procedure that preserves the tree topology and by integrating this pairing into an iterative algorithm maintaining pairing coherence. In addition, we define two complementary error measures quantifying the resulting alignment error and pairing error. Both are based on manual ground-truth that is independent of the type of transformation to retrieve.

Results: Experiments were conducted on a database of 63 clinical cases, evaluating robustness and accuracy of our approach with respect to the iterative closest point algorithm.

Conclusion: The proposed method exhibits good results both in term of pairing and alignment as well as low sensitivity to rotations to be compensated (up to 30 degrees).

Keywords Registration; Tree; Coronary Arteries; X-ray; Navigation; Iterative Closest Curve

Introduction

Percutaneous Coronary Angioplasty is mostly performed under the sole guidance of X-ray imaging. This imaging modality has rather good performance to show both the lumen of the vessels (after a selective injection of contrast medium in the arteries of interest) and the different clinical tools navigated inside patient vasculature. Main limitations includes showing the calcifications that may surround arteries and the occluded vessel sections that can occur in case of chronic total occlusion. These two characteristics have an impact on the therapeutic strategies such as the choice of stent and the pressure employed in the delivery balloon. Computed Tomography Angiography (CTA) is performed after an intra-venous injection of contrast medium and has the capability to show these elements: calcifications distribution along artery walls and characteristics of an occluded section. Thus, interventionalists may take benefit of visualizing these different imaging modalities in a common referential. To reach this goal, a step of registration is mandatory in order to provide a good alignment and relevant correspondences. This concept of taking advantage of complementary information extracted from different modalities can impact a wide variety of clinical procedures as depicted and classified in the work of [15].

Two classes of registration methods are usually distinguished [14]: feature-based and intensity-based. The latter relies on all voxels/pixels intensities and thus performs poorly when structures to be matched are sparse in both modalities. For this reason, methods based on geometrical representation (feature-based) are usually preferred in the case of vessel registration. They solve the registration problem by minimizing a cost function that quantifies the distance between two sets of features. This cost function is generally based on an underlying pairing between the two structures that may be implicit. Articles from the literature can be analyzed on the basis of the particular arrangement of the vessels to be matched.

The most popular feature-based registration algorithm is the Iterative Closest Point (ICP) because of its simplicity and the huge variety of its application fields. It has been introduced in [3] and consists of two iterated steps: 1. pairing each point of the model to its closest point in the data; 2. estimating the transformation of the model that minimizes the least squares error between paired points. Besides all its advantages, the ICP algorithm has been criticized in the literature because it

*Benseghir.Thomas@gmail.com
†Gregoire.Malandain@inria.fr
‡Regis.Vaillant@med.ge.com

necessitates a rather good initial pose estimate in order to converge to the correct solution. This limited capture range is due to the closest point assumption that creates incoherent pairing, leading to pairing "jumps" along vessels in vasculature registration (as illustrated in Fig. 3.c).

Multiple refinements of the ICP algorithm have been provided in [19], such as point-of-interest selection or pairing rejection, trying to solve the mispairing problem without changing the closest point assumption. In order to avoid the ICP to get stuck into local minima, it has been proposed in [18] to consider the closest point distance as a score function to minimize using different optimizers. The same approach is used in [16] adding a multi-scale strategy on top of the optimizer to further increase the capture range and to allow temporal registration. The original work of [7] integrates a downhill simplex optimization of the closest point distance into an Expectation-Maximization (EM) framework in order to refine the 2D segmentation and thus limit noise perturbation in the pairing. All of the above methods are based on the closest point assumption and lead to consider both vascular structures as non-connected sets of points without controlling the coherence of resulting pairings.

To diminish pairing inconsistencies, authors of [6] propose to relax the one-to-one correspondence induced by the closest point pairing to a soft assignment approach. This multiple pairings variant of ICP is equivalent to an EM-algorithm where the model point set is fitted to a probability distribution extracted from the other set of points. Similarly, works of [8, 17] consider one structure as a probability distribution changing over iterations using a deterministic annealing framework. This technique allows to progressively decreasing the "fuzzyness" of correspondences until being equivalent to an ICP method. Instead of extracting a probability function from only one point set, [1, 9] propose to consider both structures as probabilities of locations that evolve during iterations. Such technique claims to increase the capture range of standard ICP while ensuring the exact same behavior at the end of the deterministic annealing process. However, as in the "classical" ICP, the topological consistency of resulting pairings is not explicitly addressed.

Several articles take advantage of existing prior knowledge about the structure to be matched in order to build better correspondences. Assuming that a point of the model belongs to a locally curved-shape structure, a tangent vector can be extracted at each point. These local directions have been used to restrict the closest point search zone to a particular direction as in [13, 18], as well as being integrated into a mixed distance between Euclidean distance and tangent difference as in [1, 12]. Adding such local information allows to improve the geometrical consistency. However, it still does not impose coherence in the pairing as demonstrated in [12], where a penalization term is added to the optimized objective function in order to limit pairing incoherence.

Instead of penalizing incoherences in pairing between points along the same vessel, both [2, 4] consider the matching of entire vessels extracted from the main bifurcation of the 3D tree to the segmentation extremities. While [4] shows the feasibility of such an approach in clinical practice by manually providing 3D/2D vessel correspondences and segmentation, [2] proposes a framework that extends the ICP principle to curves and introduce the Iterative Closest Curve (ICC) algorithm. In addition of the general framework that provides a way to solve the problem of registering curvilinear structures, they propose a curve-pairing procedure that matches vessels starting from the main bifurcation to the segmentation extremities. By ensuring pairing coherence along vessels, both methods are going a step further in the topology preservation of the tree structure but still do not address the problem of tree matching. Actually, since main-bifurcation-to-extremities vessels are considered, matching the entire tree leads to consider multiple times the common parts without controlling explicitly their pairing coherence.

Matching tree structures has been addressed in the literature by starting to make correspondences between tree bifurcations and then aligning vessels between paired bifurcations considering them as anchor points. In the work of [20], the rigid alignment is obtained from a pairing of the tree bifurcations, then a deformation of the vessel tree centerlines is performed knowing this bifurcation pairing. The centerline location is even ignored in [22] where only the geodesic distance along them is integrated into a matrix representation of the tree. Both methods constitute an efficient and robust way to match trees when the bifurcations are sufficient to align both sets. However in the case of 3D/2D registration, obtaining a correspondence between bifurcations in both modalities, even manually, can be challenging. In fact, the projective nature of the 2D image creates superimpositions of vessels that strongly complexify bifurcation localization in 2D (in Fig. 1 the 3D bifurcations B_1, B_2 and B_3 are projected into the same area and correspond to the node n_1 in the 2D image). In addition, the right coronary tree of some patients may be quite poor in term of number of bifurcations (may fall down to 2 or 3) which forbids even a 3D rigid alignment.

Inspired from the work of [20] on tree matching, we propose a pairing procedure which preserves the tree topology of the model but without assuming that correspondences can be made between bifurcations of the two modalities, since their precise identification in 2D is usually not achievable. Instead of ignoring centerlines as in the matching process described in [20], that is only based on bifurcation matching, the pairing pro-

cedure described in this article matches tree centerlines while ensuring connectivity at bifurcation points. We integrate the proposed pairing procedure into the framework designed to register curves, introduced in [2], by replacing their pairing procedure by our tree-preserving one. Contrary to [2] that considered the pairing of proximal vessels multiple times without any control on the coherence, the proposed approach ensures a one-to-one matching of curves (and points) in the model while preserving the tree topology. By imposing such consistency, we expect the resulting pairing to be more relevant regarding the clinical application. The resulting registration algorithm is applied to a dataset of 63 clinical cases extracted from 13 different patients. The registered transformation and pairing are evaluated using two dedicated error measures built upon a manually obtained Ground-Truth (GT) that endorses the correct correspondence between vessels of the two modalities.

Material and Motivation

Topology preservation is the core of our work, thus let us start by describing in detail the two vascular structures to be registered. The 3D information is extracted from a Computed Tomography Angiography (CTA) scan by a fully automated commercial product (Volume Viewer, GE-Healthcare) providing an automatic segmentation of the coronary vessel tree of the patient as shown in Fig. 1. This segmentation can be represented by 3D centerlines (blue curves in the top row of Fig. 1) linked to each other at bifurcation points (blue dots in Fig. 1). Each centerline is modeled as a polygonal curve $C = [C[1] \dots C[\#]]$ in the 3D space, where $C[\#]$ denotes the end point of the curve. A parenthood relation can be defined in this vessel tree structure: starting from the root centerline R, the curves C_1 and C_2, connected to R via the bifurcation point B_1 (main bifurcation), are called child centerlines of R (see Fig. 1). Recursively, a hierarchy between centerlines $\mathbf{C}$ and bifurcations $\mathbf{B}$ can be defined, forming a rooted-tree structure $\mathcal{Y} = (\mathbf{C}, \mathbf{B})$ where edges correspond to 3D centerlines and nodes to 3D bifurcations. From a topological point of view, a tree presents two types of connectivities: 1) connectivity between points that belong to the same centerline curve; 2) connectivity between centerlines extremity points induced by a shared bifurcation. Both properties are important to preserve during the pairing procedure. Another interesting property of the tree is that it can be recursively divided into several subtrees. For example, in Fig. 1, the root R has two child subtrees $\mathcal{Y}_{C_1}$ and $\mathcal{Y}_{C_2}$.

After a step of vessel enhancement (using a Hessian-based technique [10]), 2D features are extracted from the fluoroscopic image that can be gathered in a structured representation (Fig. 1 bottom row). Similarly to the model representation, it is composed of 2D centerlines linked by each other at bifurcation points. However, because of the projective nature of the 2D modality, "fake" bifurcations that are created by vessel superimpositions can appear in the image (e.g. node n_5 in Fig. 1 last column bottom row). Therefore, the 2D structure is represented by a graph $\mathcal{X} = (\mathbf{c}, \mathbf{n})$, instead of a tree, that is composed of a set of edges $\mathbf{c}$ and nodes $\mathbf{n}$ respectively corresponding to centerline curves and bifurcation points. Contrary to the pre-operative 3D modality, which is used for diagnosis and planning purpose, the 2D graph is extracted intra-operatively and is not intended to be edited by the clinician. For this reason, the 2D graph structure $\mathcal{X}$ is subject to noise and false detection. We will consider it as the *data* in contrast to the 3D tree $\mathcal{Y}$ that can be manually corrected during the planning and will be referred as the *model*.

Fusing the two previous modalities refers to the problem of 3D/2D registration. It is generally expressed as finding the transformation $\hat{T}$ of the model $\mathcal{Y}$ that best aligns it with respect to the data $\mathcal{X}$:

$$\hat{T} = \underset{T}{\operatorname{argmin}} \left\{ \mathcal{D}\big(P \circ T\left(\mathcal{Y}\right), \mathcal{X}\big) \right\} \tag{1}$$

where T belongs to the set of admissible transformations (in our case rigid transformations), $\mathcal{D}$ quantifies the distance between the two structures to be registered and P is the projective operator that is mandatory to compare a 3D and a 2D modality. The matrix P as well as an initial estimate of the registration transformation T_0 are provided by the system calibration. Generally, the distance $\mathcal{D}$ is based on a set of pairings, that can be either explicit or implicit, between the two structures to be matched. In the case of model-to-data registration, the pairing set is made in a non-symmetrical way, seeking for correspondents of model points in the data.

We propose to build a *tree-pairing* set that preserves the two types of connectivities characterizing the tree topology of the model. However, contrary to the work of [20] we get rid of the strong assumption that a bifurcation in the model corresponds to a bifurcation in the data. First, an edge of the model tree (a 3D centerline) must be matched to a path p in the data graph. We define a path in the graph as a walk (sequence of nodes and edges pairwisely connected) that can start and end either on a graph node or along an edge. Moreover, two 3D edges connected by a given bifurcation must be paired to 2D paths that are also connected (i.e. their union is also a path in the graph). By imposing these two conditions, we preserve the tree topology during the pairing procedure. The resulting tree-pairing Π is composed of elements (C, p) that associate a 3D centerline edge C and a 2D centerline path p. The way to obtain such pairing is one of the major contribution of this paper and will be described in Sec. .

Such tree-pairing procedure can be easily introduced

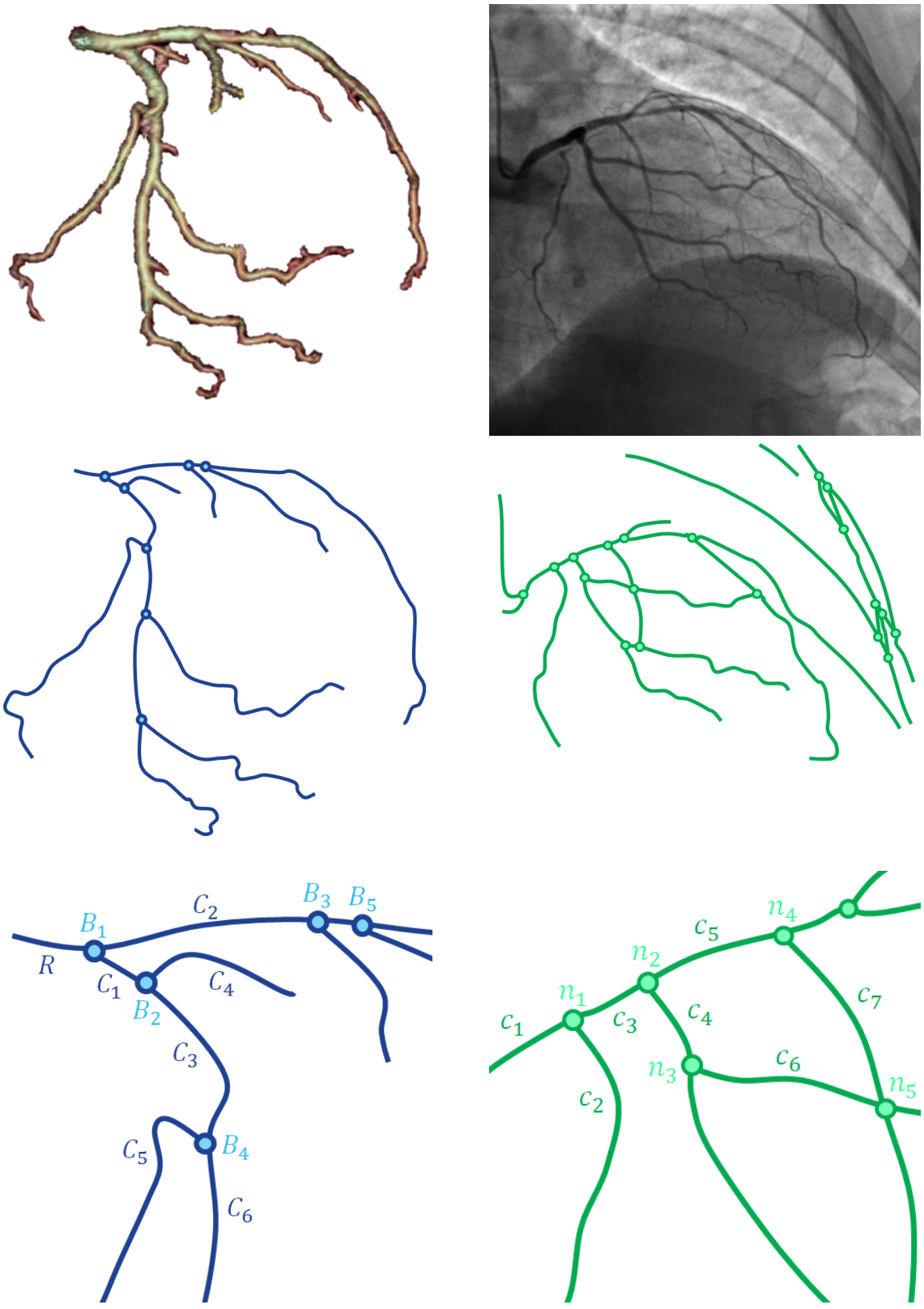

Figure 1: Structures to be registered. The first column corresponds to the 3D modality and the second column to the 2D modality. The first row refers to native clinical representation, the second to extracted sparse geometric structures and the third to a zoom on the proximal part.

into the Iterative Closest Curve (ICC)-framework introduced in [2]. It aims at solving the registration problem of (1) where the distance $\mathcal{D}$ is based upon curve-pairings instead of point-pairings. The ICC algorithm iteratively alternates the curve-pairing procedure at a given transformation estimation and the transformation optimization given the previous pairing. Given a 3D/2D tree-pairing Π, the second step of this method consists in optimizing with respect to T the objective function:

$$\mathcal{D}\big(P \circ T\left(\mathcal{Y}\right), \mathcal{X}\big) = \sum_{(C,p)\in\Pi} \mathcal{F}(P \circ T(C), p)^2 \quad (2)$$

where $\mathcal{F}(.,.)$ denotes the discrete Fréchet distance that measures the distance between two polygonal curves. Introduced in [5], it is based on an underlying point-pairing set which preserves point order along curves. Thus, the step that estimates the transformation in the ICC-framework aims at best aligning a set of paired curves taking into account connectivity between points along those curves.

Tree-Topology Preserving Pairing Procedure

As described in Sec. , we aim at building correspondences between the 3D model and the 2D data that enforce tree-topology preservation. We propose to solve this tree-matching problem by choosing the best curve-pairing set $\hat{\Pi}$, regarding a global pairing score $\bar{S}$, among the set of all possible tree-pairings $\Omega\left(\mathcal{Y}\right)$:

$$\hat{\Pi} = \underset{\Pi\in\Omega(\mathcal{Y})}{\operatorname{argmax}}\, \bar{S}\left(\Pi\right) \quad (3)$$

The pairing score $\bar{S}$ is designed to quantify the quality of a curve-pairing set and will be properly defined in Sec. . Regarding the set of possible tree-pairings $\Omega\left(\mathcal{Y}\right)$, let us give to the reader an intuition on how to build one of its elements using the example of Fig. 1.

We assume that the root centerline R can only be paired to the path p_R composed of the single 2D centerline c_1. Because of the connectivity constraint at bifurcation B_1, all 3D child centerlines of R must be paired to paths in the graph that are connected to the extremity point of p_R corresponding to B_1 (in this case the node b_1 in Fig. 1). Thus, the child centerline C_1 cannot be paired to c_7 but could be paired for example to $p_1 = c_3$ or to $p_1' = [c_2[1] \dots c_2[10]]$, which is the path composed of the ten first points of the centerline c_2. The latter denotes a path in the graph that ends along a centerline and not at a bifurcation node. One has to note that choosing the path p_1 instead of path p_1' will impact the possible pairings of the child centerlines of C_1 because of the connectivity constraint. Keeping this example in mind, one can build a tree-pairing for general cases by following the recursive heuristic: 1. pairing the root of the tree to a path in the graph from a set of selected candidates; 2. building the pairing of each child subtree imposing the connectivity preservation accordingly to the root pairing.

Now that we are able to build a given pairing, we aim at choosing the best among them. In one hand, since choosing a candidate for a given centerline impacts potential pairings of all of its children, an a-priori choice of the best candidate seems irrelevant. In the other hand, solving (3) by an exhaustive evaluation of every possible curve-pairing sets in $\Omega\left(\mathcal{Y}\right)$ becomes intractable in practical situation. To overcome this issue, we propose a divide-and-conquer algorithm based on a recursive decomposition of the optimal tree-pairing problem into subproblems. Even if such approach reduces drastically the complexity with respect to an exhaustive search approach, several other refinements are proposed to control the computational time.

Candidate Selection

In this section, we aim at finding paths in the data graph $\mathcal{X}$ that could be matched to a model tree centerline C. To be considered as a candidate, a path p extracted from the graph must first preserve connectivity with the path paired to the parent centerline of C in the tree. This constraint is carried by a point-pairing between the parent bifurcation of C, denoted B, and a point b along the graph structure. We express at the end of this section how this pairing is obtained to continue the recursion and how it is initiated for the root centerline. Thus, the starting point $p[1]$ of path p must be the point b itself. Regarding the ending point $p[\#]$, it is expected to be close to the projection of the end extremity $C[\#]$ of C, which can be formalized as being included in the 2D neighborhood centered in $P(C[\#])$ of radius R_C, denoted $\mathcal{N}(P(C[\#]), R_C)$.

We propose to consider all paths p extracted from the graph $\mathcal{X}$ such that $p[1] = b$ and $p[\#]$ belongs to $\mathcal{N}(P(C[\#]), R_C)$. Instead of only computing the shortest path in the 2D graph as in [2], we found more realistic to look for all 2D paths having a length that is compatible with the projection of the 3D curve. Thus, the length difference $|\mathcal{L}\left(P(C)\right) - \mathcal{L}(p)|$ should be smaller than an expected variation ΔL_C. The main contributor of such difference in length is the degree of alignment between the vessel C and the projection axis called the *projective foreshortening*. The more a vessel is aligned along the direction of projection the shorter it will appear on the 2D image plane and the larger will be its potential length variation ΔL_C for a small perturbation in rotation.

Using all previous criteria, we define the set of candidates that are compatible with the model curve C given the starting point pairing (B, b), denoted $\Gamma\left(C \mid (B, b)\right)$,

by the following equation:

$$p \in \Gamma\Big(C \mid (B,b)\Big) \Leftrightarrow \begin{cases} p[1] = b \\ p[\#] \in \mathcal{N}\left(P(C[\#]), R_C\right) \\ \big|\mathcal{L}\big(P(C)\big) - \mathcal{L}(p)\big| < \Delta L_C \end{cases} \quad (4)$$

To run the recursive pairing on the whole tree, one must provide the end point-pairing relative to the child bifurcation B' of C for a candidate p. We propose to use the final element of the point-pairing set induced by the discrete Fréchet distance to initiate children recursive call.

Implementation details: The previous candidate selection assumes that a point pairing is provided for the parent bifurcation. In order to initiate this process for the root centerline, we assume that the point pairing of main bifurcation of the tree (B_1 in the example of Fig. 1) is provided as initialization of the pairing algorithm. In practice, it can either be obtained by a single click user interaction, an automated detection as in [11] or by trying multiple initial hypotheses. Regarding the radius R_C of the extremity search neighborhood, we assume that it is proportional to the distance between the main bifurcation and the 3D extremity of the centerline C. Actually, the main bifurcation initialization gives a coarse in-plane translation alignment of the model proximal part but becomes less precise with the distance to this anchor point.

Pairing Score

In order to choose the best tree-pairing among all and thus solve (3), we define a pairing score $\bar{S}(\Pi)$ relative to a tree-pairing Π. This score is based on a sum of curve-pairing scores weighted by the length $\mathcal{L}(C)$ of each curve C:

$$\bar{S}(\Pi) = \sum_{(C,p)\in\Pi} \mathcal{L}(C) \cdot S\big(C,p\big) \quad (5)$$

The curve-pairing score S quantifies the quality of a 3D/2D curve-pairing (C,p) and is based on two criteria that quantify their geometric distance and their resemblance. The first criterion corresponds to a common assumption made in matching procedure: the closer, the better. The more a 3D curve projection $P(C)$ is close to its pairing candidate p, the more likely such matching is to be correct. It can be computed using the discrete Fréchet distance previously mentioned in (2) by:

$$F(C,p) = \mathcal{F}(P \circ T(C), p) \quad (6)$$

where T denotes the current estimate of the transformation in the registration process. This geometric distance is natural to consider but the literature highlighted the importance of completing it with shape information in order to increase the correct pairing success rate.

However, instead of using local information, such as tangent vector or curvature as in [1, 12, 21], which are not relevant in highly foreshortened vessel portions, we aim at quantifying the resemblance between two curves globally. We designed a shape resemblance measure mimicking the human eye behavior: "Two curves have similar shapes if a rigid transformation can align them with a small registration error". Since the 3D-to-2D registration problem may become highly ill-posed for only one pair of curves, we propose to register the projection of C to p in the image plane. This sub-problem can be solved using a 2D-ICP-like procedure where closest point pairing is replaced by the point-pairing induced by the Fréchet distance $\mathcal{F}$. We denote $\hat{T}_{2D}$ the optimal rigid 2D transformation obtained at convergence of this procedure that consists in iterating the Fréchet pairing and the least squares transformation estimation. The curve resemblance $R(C,p)$ can be quantified by the residual Fréchet distance at this 2D registered position:

$$R(C,p) = \mathcal{F}\left(\hat{T}_{2D} \circ P \circ T(C), p\right) \quad (7)$$

where a resemblance of 0 corresponds to a perfect match.

We define the overall curve-pairing score $S(C,p)$ by:

$$S(C,p) = \alpha \cdot e^{-\frac{F(C,p)^2}{2{\sigma_F}^2}} + (1-\alpha) \cdot e^{-\frac{R(C,p)^2}{2{\sigma_R}^2}} \quad (8)$$

where $\alpha \in [0;1]$ controls the relative importance of the two characteristics, and σ_F and σ_R are used to normalize both criteria. Using (8), the tree-pairing score of (5) can be computed in order to evaluate the quality of different tree-pairing possibilities.

Pairing Algorithm

Now that we can quantify the quality of a curve-pairing set, we aim at finding the best pairing above all tree-pairing possibilities $\Omega(\mathcal{Y})$ by solving (3). As discussed in Sec. , the main bifurcation pairing is mandatory to initiate the candidate selection and thus restrict the set of possible pairings, which is now denoted $\Omega(\mathcal{Y} \mid (B,b))$. An element Π of this set can be decomposed into:

$$\Pi = \{(R,p)\} \cup \Pi_{C_1} \cup \Pi_{C_2} \ldots \quad (9)$$

where R denotes the root centerline, p must belong to $\Gamma(R \mid (B,b))$ and thus respects the connectivity constraint imposed by the main bifurcation pairing (B,b), and finally Π_{C_1}, resp. Π_{C_2}, is the subtree pairing extracted from Π that is relative to the child subtree $\mathcal{Y}_{C_1}$, resp. $\mathcal{Y}_{C_2}$. We denote $(B', {b_p}')$ the child bifurcation point-pairing induced by the root curve-pairing (R,p). Therefore, Π_{C_1} must belong to $\Omega\left(\mathcal{Y}_{C_1} \mid (B', {b_p}')\right)$, and Π_{C_2} must belong to $\Omega\left(\mathcal{Y}_{C_2} \mid (B', {b_p}')\right)$, because of the connectivity constraint at bifurcation location.

The separability of the pairing-score into independent curve-pairing scores, expressed in (5), allows us to obtain the following relation:

$$\bar{S}\left(\Pi\right) = \mathcal{L}(R) \cdot S\left(R, p\right) + \bar{S}\left(\Pi_{C_1}\right) + \bar{S}\left(\Pi_{C_2}\right) \dots \quad (10)$$

Then, referring to (3) and using (9) and (10), we are able to obtain:

$$\max_{\Pi} \bar{S}(\Pi) = \max_{p} \Big\{ \mathcal{L}(R) \cdot S\left(R, p\right) + \max_{\Pi_{C_1}} \bar{S}\left(\Pi_{C_1}\right) + \max_{\Pi_{C_2}} \bar{S}\left(\Pi_{C_2}\right) \dots \Big\} \quad (11)$$

subject to:

$$\begin{cases} \Pi \in \Omega\left(\mathcal{Y} \mid (B, b)\right) \\ p \in \Gamma\left(R \mid (B, b)\right) \\ \Pi_{C_i} \in \Omega\left(\mathcal{Y}_{C_i} \mid (B', {b_p}')\right) \end{cases} \quad (12)$$

where i indexes the different children of R. From (11) we showed that the problem of finding the optimal tree-pairing for the whole tree $\mathcal{Y}$ involves to find an optimal subtree-pairing for each child subtree. This property of breaking down a problem into simpler subproblems is known in the literature as an *optimal substructure* and can be directly implemented into a recursive algorithm.

In order to restrict the computational cost in case of noisy segmentation, which leads to increase of the number of possible candidates in $\Gamma(.)$, we propose two different refinements. First, we already noted that the set of possible pairings for a given child subtree depends on the parent centerline end point pairing. Thus, if two paths p and p' are two compatible candidates in $\Gamma(.)$ that leads to the same child bifurcation pairing, then they will generate the same set of possible pairings for each child-subtree. In other word, the candidate that will give the best score can be chosen only on the elementary scores $S\left(C, p\right)$ and $S\left(C, p'\right)$.

The second trick used to manage the algorithm complexity is to limit the number of candidates in $\Gamma(.)$. In practice, the set $\Gamma(.)$ can be composed of several similar curves that only differs from each other in a small area where the graph structure complexity increases due to fake centerline detection. Such multiplicity impacts a lot the computation time but not much the resulting pairing. We therefore decided to restrict the set $\Gamma(.)$ to at most N elements, by choosing the most relevant ones based on their elementary pairing score and their redundancy with respect to other candidates. The redundancy is estimated by the intersection of the ordered-point-sets constituting the candidate curves. This restriction of the set $\Gamma(.)$ can be seen as a stopping condition which is used to control computational time.

Registration Quality Evaluation

For a clinical fusion application, a 3D/2D registration algorithm must not only provide a good alignment between projected vessels and their correspondents in the image but also a meaningful mapping between both modalities. In the following, we propose two different measures evaluating both aspects and show their accordance with respect to a visual evaluation. These measures are based on a proposed ground-truth (GT) definition which is independent of the presence of landmarks, anatomical or surgically implanted, and of the nature of the transformation to be compensated (rigid, affine...). Based on this same manual GT definition, we build both error measures taking into account the tree structure of the model.

An ideal ground-truth (GT) would provide dense correspondences between 3D points composing the 3D tree model and points in the image plane. However, contrary to synthetic data, such GT is not conceivable to obtain for clinical cases. Other approaches are based on sparse point correspondences of anatomical landmarks identified in both modalities. In the case of vessel registration, such landmarks can correspond to either vessel tree bifurcations or particular anatomy tortuosities. Both are challenging to identify in the projective image because they induce by nature superimposition of multiple vessels in the image. To overcome the problem of anatomical points correspondences, several authors [1, 18] propose to identify the whole 2D vessel structure corresponding to the segmented 3D model in order to build a distance between two sets of points. Inspired from them, we extend their GT definition by associating to each manually marked 2D vessel its 3D counterpart in the model. This task can be handled by a trained observer.

In order to avoid the problem of bifurcations localization, we propose to identify in both modalities corresponding centerline paths departing from the tree main bifurcation and ending at a vessel extremity (limit of visibility in one of the two modalities). In model-to-data registration, the model is regularly used as GT since it has already been validated by an expert. For each 3D model vessel W_q linking the main bifurcation to a leaf extremity, the observer identifies the corresponding 2D curve w_q by marking several successive points in the 2D image (see Fig. 3.a). The proposed GT is a set of 3D/2D curve pairing (W_q, w_q) which represents all observable vessels from the main bifurcation to extremities that can be identified in both modalities. If a vessel is not visible in the image because of occlusion or out of field of view reasons, it is ignored from the GT definition. GT curve-pairing will allow us to define error measures taking into account the vessel structure of both modalities. However it also induces some redundancy since proximal centerlines can contribute to several paths W_q. This point is addressed in the upcoming error measures by considering that the common part of multiple GT 3D vessels must be close to *every* corresponding GT 2D vessels. Based on this assump-

tion, we are able to take into account the tree structure of the data while avoiding the challenge of localizing bifurcations.

As mentioned earlier, we want to assess the quality of the two crucial outputs of a registration algorithm: the transformation $\hat{T}$ and the pairing $\hat{\pi}$ using this proposed GT. In the following we will consider error measures as summations over all points constituting the model $\mathcal{Y}$. This choice is based on the model-to-data nature of the problem and corresponds to standards adopted in the literature. Regarding the alignment error ε_A, most of state of the art articles on 3D-2D vessel registration compute the Mean Projective Error (MPE), considering the GT as two sets of points with no particular structure arrangement. The previous GT definition allows us to quantify if a vessel is close to its correct correspondent and not only close to the overall structure. A point Y in the 3D tree may belong to several 3D GT curves W_q's. We identify all pairs (W_q, w_q) such that $Y \in W_q$ and consider for Y the worst projective error over all pairs (W_q, w_q). Hence, we propose the following formulation of the transformation error:

$$\varepsilon_A = \frac{1}{\text{card}(\mathcal{Y})} \sum_{Y \in \mathcal{Y}} \max_q \left\{ d\Big(P \circ \hat{T}(Y), w_q\Big) \mathbb{1}_{W_q}(Y) \right\} \tag{13}$$

where $\mathbb{1}_{W_q}$ is the indicator function of the 3D GT curve (equals one if a point is along the curve and 0 otherwise), and $d(., w_q)$ is the usual 2D Euclidean distance distance with respect to the curve w_q.

The previous measure quantifies the quality of the resulting transformation by computing the average distance between the projection of a transformed model point and the 2D vessel portion where it should be close to. We propose to apply the same principle to the resulting pairing set $\hat{\pi}$ in order to build the pairing error ε_P. It is made of several 3D/2D point-pairings (Y, x) making correspondence between a point in the model $\mathcal{Y}$ and a data point along $\mathcal{X}$. For all pairs (W_q, w_q) such that $Y \in W_q$, we expect x to be close to w_q. In other word, the quality of the pairing (Y, x) depends on the following quantity:

$$\delta(Y, x) = \max_q \left\{ d\left(x, w_q\right) \mathbb{1}_{W_q}(Y) \right\} \tag{14}$$

By summing over all the pairings, one is able to obtain a pairing error that is the exact twin of the alignment error of (13) using paired points instead of projected ones. However, a pairing is more judged as correct or wrong than as close or far from the target. We thus propose to define the pairing error ε_P as:

$$\varepsilon_P = \frac{1}{\text{card}(\hat{\pi})} \sum_{(Y,x) \in \hat{\pi}} \mathbb{1}_{[0;D]}\left(\delta(Y, x)\right) \tag{15}$$

where D controls the accuracy expected for the clinical application and is set to the typical diameter of the coronary arteries (about 3mm).

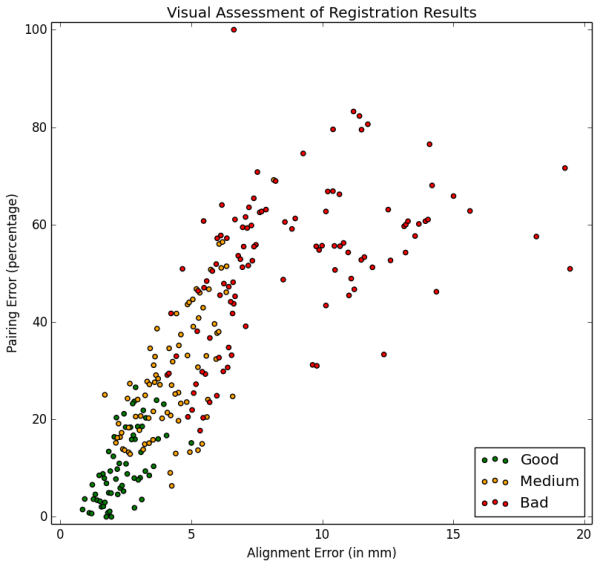

Figure 2: Correlation of the two quality measures with respect to visual assessment.

The relevance of these two new error measures has been validated by visually assessing the quality of 200 registration results on different patients and angulations. A trained observer classified them into three categories based on the registration algorithm outputs: good, medium, and bad registration. Results are presented in Fig. 2, highlighting good correlation between the two measures and this visual assessment. The lower the alignment error and pairing error, the more likely a registration result is to be relevant for guidance. Boundaries between the different registration quality classes in the $(\varepsilon_A, \varepsilon_P)$-plane cannot be simply defined by applying a threshold to any of these two error measures. This last point reinforces the complementarity of the two error measures.

Results

We evaluate our tree-topology preserving version of the Iterative Closest Curve algorithm (simply referred in the following as TP-ICC) using a dataset of 63 clinical cases. This database is formed of clinical images collected at hospital sites in the context of standard of care procedures. Appropriate patient consents have been collected by physicians to include these images, after being anonymized, in this research project. A case is composed of a 3D automatic segmentation of the coronary tree, an automatic segmentation of the fluoroscopic image (extracted from an injected run at the same cardiac cycle as the one where the CTA-scan has been acquired), and the calibrated position of the C-arm system providing the 2D image. Each case has been extracted from 13 different patients suffering from

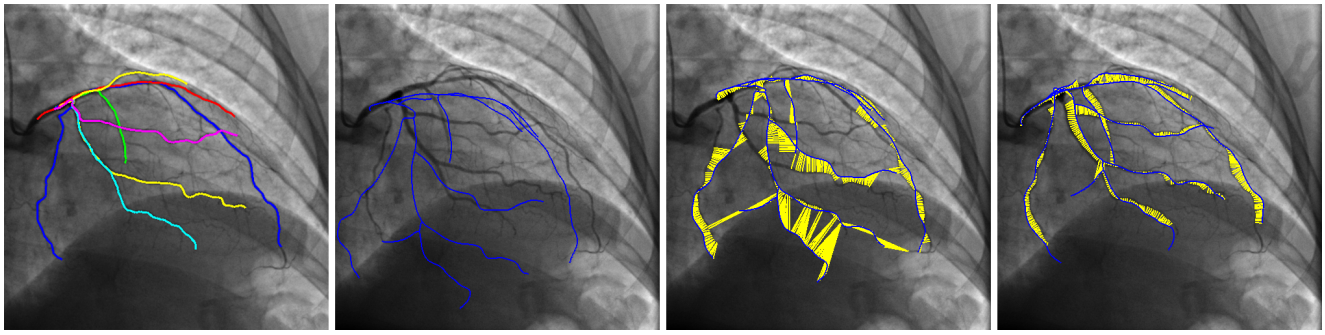

Figure 3: From left to right: a) manually defined 2D ground-truth, b) 3D model initial pose projection (blue) estimated by calibration, c) ICP registered pose projection (blue) with resulting pairings (yellow), d) TP-ICC registered pose projection (blue) with resulting pairings (yellow).

different kinds of pathologies that impact the left or the right coronary tree. Several cases are extracted from a same patient considering either a different side of the tree (left or right) or a different angulation of the X-ray view.

The first experiment is conducted under standard clinical conditions, where the patient's relative positions between pre- and intra-operative states are unknown. In addition to the system calibration, which allows one to set the 3D volume at the interventional system isocenter with a similar patient's orientation, the initial pose estimate is set using the 2D location of the root given by the clinician which corresponds to a coarse in-plane translation initialization. Starting from this position both the previously described TP-ICC and an ICP algorithm were run, seeking for a rigid transformation. We assess the accuracy of these two algorithms on all the 63 cases by computing both the alignment error and the pairing error defined in Sec. and summarize it in two box-plots comparisons provided in Fig. 4. Both resulting pairing sets used to compute the pairing error are the point-pairing sets induced by the registration distance of (2) (closest point pairing for ICP and Fréchet pairing for TP-ICC). While the better performance in term of geometrical alignment of the TP-ICC with respect to the ICP is not revealed by a t-test (p-value of 0.22), its superiority in term of topological alignment (ie pairing) is statistically significant (p-value of 0.0004). Thus, by imposing topology preservation during the pairing procedure, the resulting correspondences between the model and the data are significantly more coherent than using the closest point assumption. While the ICP-algorithm get stuck in the position presented in Fig. 3.c because of multiple pairing jumps, the coherence induced by our approach allows the TP-ICC algorithm to converge to the correct solution presented in Fig. 3.d.

In order to compare the robustness of both the ICP and TP-ICC methods, we propose to apply random perturbations of a reference registration transformation T_{Ref} obtained using the manually defined ground-truth. By iterating an ICP-like approach using the pairing defined in (13), we were able to compute the transformation T_{Ref}. Starting from these individual reference positions, 150 random additional perturbations are applied to each case. Each perturbation is modeled by a rotation of uniform random axis and uniform random angle (between 0 and 30 degrees) applied around the model main bifurcation. The distribution study of T_{Ref} on the whole database showed uniform repartition between 0 and 20 degrees, which has been extended to 30 in this experiment in order to study the behavior of both algorithms in a full range of conditions.

Results are grouped with respect to the rotation angle and presented in Fig. 5. The non-significant difference for small angles confirms the accuracy characteristic of the ICP method, and thus the TP-ICC, when the initial position is close to the solution. However, the coherence imposed by the TP-ICC algorithm results in much better performances than its ICP counterpart for larger angles, in both alignment error and pairing error. Introducing global coherence in the pairing procedure results in a much more robust algorithm while maintaining accuracy.

Discussion and Conclusion

Integrating vessel calcifications and occlusion characteristics, revealed in the pre-operative CTA, into the live fluoroscopic image can greatly improve guidance in percutaneous coronary interventions. Such application necessitates a step of registration that must provide relevant correspondences between these two complementary modalities. In order to avoid incoherences in the vasculature matching, we proposed a registration algorithm which endorses the tree nature of the reference 3D structure. It is achieved by integrating a pairing procedure, that preserves tree topology, into the Iterative Closest Curve (ICC) framework which allows us to maintain this pairing coherence along the registration. The main

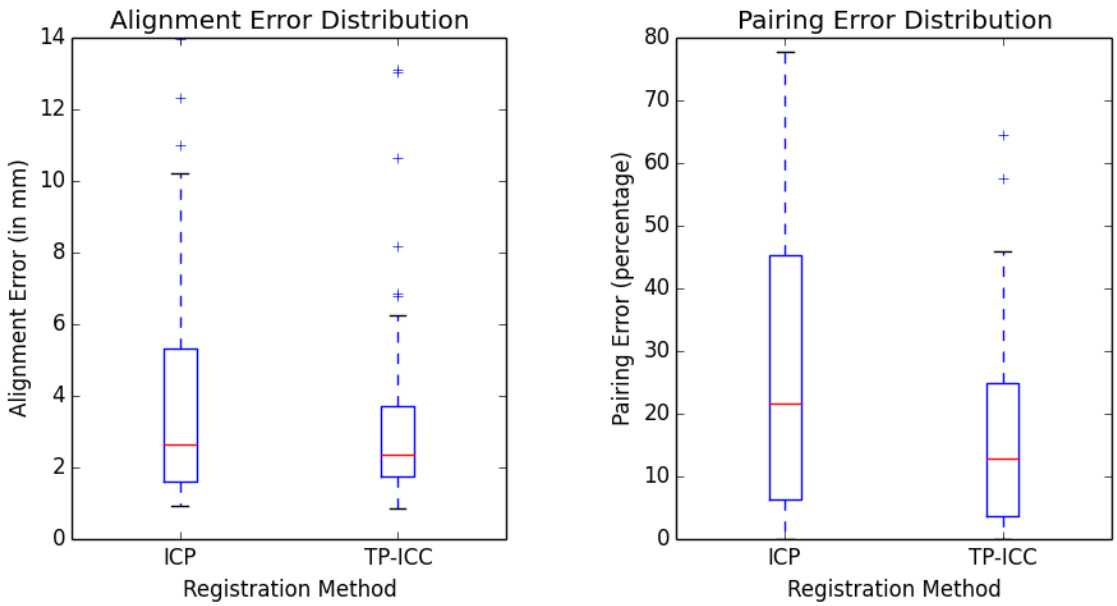

Figure 4: Real conditions experiment results: box-plots comparison of ICP and TP-ICC of the two ground-truth based error measures (left: alignment error, right: pairing error)

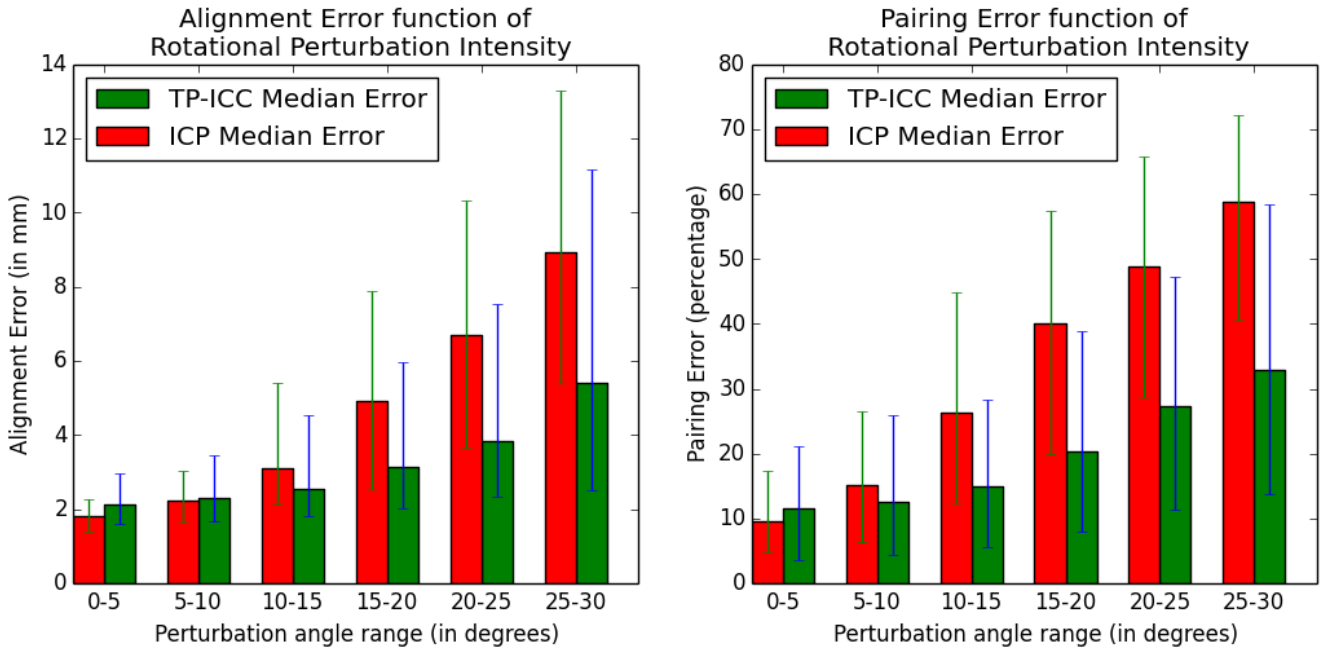

Figure 5: Robustness study: error median values for different ranges of perturbation angles for ICP (red) and TP-ICC (green). Vertical segments corresponds to the 25th percentile (lower) and the 75th percentile (higher)

challenge consisted in finding the optimal tree-pairing, in the sense of a dedicated pairing-score, above all tree-topology preserving possibilities. It can be solved efficiently by a divide and conquer algorithm based on the optimal substructure nature of the problem. The evaluation of this algorithm is performed on 63 clinical cases comparing its robustness and accuracy with respect to the Iterative Closest Point (ICP) algorithm. We show the performance of our approach in term of resulting alignment and pairing using two error measures based on a manual Ground-Truth that is independent of the transformation to retrieve.

These two complementary error measures allow one to judge if a case could benefit from a non-rigid alignment. If a registration result presents both a low pairing error and a relatively high alignment error, then extending our approach from rigid to non-rigid registration should have a great impact on such case. In addition, because coherence is enforced by the proposed pairing procedure, no extra regularization term is expected to avoid non-plausible transformations as it is generally the case in the literature. As highlighted in [2], several variants of the ICP algorithm, such as outlier rejection or expectation maximization versions, can be extended to the ICC framework in order to further increase robustness and accuracy. Our method is directly applicable to other feature-based 3D/2D vessel registration problems, such as liver or neurology application. While an extension to 3D/3D tree registration seems quite straightforward, the applicability to 2D graph matching is still an open question. Finally, the recursive nature of the matching problem can easily lead to a parallelized implementation which can greatly decrease the 180 seconds average computational time obtained on an Intel CORE i5 cadenced at 1.5 GHz (ICP took around 5s).

References

[1] Baka, N., Metz, C.T., Schultz, C.J., van Geuns, R.J., Niessen, W.J., van Walsum, T.: Oriented gaussian mixture models for nonrigid 2d/3d coronary artery registration. IEEE Transactions on Medical Imaging **33**(5), 1023–34 (2014)

[2] Benseghir, T., Malandain, G., Vaillant, R.: Iterative closest curve: A framework for curvilinear structure registration application to 2d/3d coronary arteries registration. In: Medical Image Computing and Computer-Assisted Intervention - MICCAI 2013, vol. 8149, pp. 179–186 (2013)

[3] Besl, P., McKay, N.: A method for registration of 3-d shapes. IEEE Transactions on Pattern Analysis and Machine Intelligence **14**(2), 239–256 (1992)

[4] Duong, L., Liao, R., Sundar, H., Tailhades, B., Meyer, A., Xu, C.: Curve-based 2d-3d registration of coronary vessels for image guided procedure. In: SPIE, vol. 7261 (2009)

[5] Eiter, T., Mannila, H.: Computing discrete fréchet distance. Tech. rep., Christian Doppler Laboratory for Expert Systems, TU Vienna, Austria (1994)

[6] Granger, S., Pennec, X.: Multi-scale em-icp: A fast and robust approach for surface registration. In: European Conference on Computer Vision, vol. 2353, pp. 418–432 (2002)

[7] Groher, M., Bender, F., Hoffmann, R.T., Navab, N.: Segmentation-driven 2d-3d registration for abdominal catheter interventions. In: Medical Image Computing and Computer-Assisted Intervention - MICCAI 2007, vol. 4792, pp. 527–535 (2007)

[8] Groher, M., Zikic, D., Navab, N.: Deformable 2d-3d registration of vascular structures in a one view scenario. IEEE Transactions on Medical Imaging **28**(6), 847–860 (2009)

[9] Jian, B., Vemuri, B.: Robust point set registration using gaussian mixture models. IEEE Transactions on Pattern Analysis and Machine Intelligence **33**(8), 1633–1645 (2011)

[10] Krissian, K., Malandain, G., Ayache, N., Vaillant, R., Trousset, Y.: Model-based detection of tubular structures in 3D images. Computer Vision and Image Understanding **80**(2), 130–171 (2000)

[11] Lacroix, R., Florent, R., Auvray, V.: Model-based segmentation of the left main coronary bifurcation from 2d angiograms. In: IEEE International Symposium on Biomedical Imaging (ISBI), 2012 9th, pp. 780–783. IEEE (2012)

[12] Lee, J.H., Won, C.H.: Topology preserving relaxation labeling for nonrigid point matching. IEEE Transactions on Pattern Analysis and Machine Intelligence **33**(2), 427–432 (2011)

[13] Liu, A., Bullitt, E.: 3d/2d registration via skeletal near projective invariance in tubular objects. In: Medical Image Computing and Computer-Assisted Interventation - MICCAI 98, pp. 780–787 (1998)

[14] Maintz, J., Viergever, M.: A survey of medical image registration. Medical Image Analysis **2**(1), 1–36 (1998)

[15] Markelj, P., Tomaževič, D., Likar, B., Pernuš, F.: A review of 3d/2d registration methods for image-guided interventions. Medical Image Analysis **16**(3), 642–661 (2012)

[16] Metz, C.T., Schaap, M., Klein, S., Baka, N., Neefjes, L.A., Schultz, C.J., Niessen, W.J., Walsum,

T.V.: Registration of 3d+t coronary cta and monoplane 2d+t x-ray angiography. IEEE Transactions on Medical Imaging **32**(5), 919–931 (2013)

[17] Myronenko, A., Song, X.: Point set registration: Coherent point drift. IEEE Transactions on Pattern Analysis and Machine Intelligence **32**(12), 2262–2275 (2010)

[18] Rivest-Henault, D., Sundar, H., Cheriet, M.: Non-rigid 2d/3d registration of coronary artery models with live fluoroscopy for guidance of cardiac interventions. IEEE Transactions on Medical Imaging **31**(8), 1557–1572 (2012)

[19] Rusinkiewicz, S., Levoy, M.: Efficient variants of the icp algorithm. In: Third International Conference on 3-D Digital Imaging and Modeling, pp. 145–152. IEEE (2001)

[20] Serradell, E., Pinheiro, M., Sznitman, R., Kybic, J., Moreno-Noguer, F., Fua, P.: Non-rigid graph registration using active testing search. IEEE Transactions on Pattern Analysis and Machine Intelligence **37**(3), 625–638 (2015)

[21] Serradell, E., Romero, A., Leta, R., Gatta, C., Moreno-Noguer, F.: Simultaneous correspondence and non-rigid 3d reconstruction of the coronary tree from single x-ray images. In: International Conference on Computer Vision 2011, pp. 850–857 (2011)

[22] Smeets, D., Bruyninckx, P.: Robust matching of 3d lung vessel trees. In: MICCAI Workshop on Pulmonary Image Analysis, vol. 2, pp. 61–70 (2010)